AIAA 94-0561

Effects of Initial Flow Conditions on Primary Breakup of Nonturbulent and Turbulent Liquid Jets

P.-K. Wu, R. F. Miranda and G. M. Faeth
The University of Michigan
Ann Arbor, MI

32nd Aerospace Sciences Meeting & Exhibit
January 10-13, 1994 / Reno, NV

EFFECTS OF INITIAL FLOW CONDITIONS ON PRIMARY BREAKUP OF NONTURBULENT AND TURBULENT LIQUID JETS

P.-K. Wu,* R.F. Miranda† and G.M. Faeth**
Department of Aerospace Engineering
The University of Michigan
Ann Arbor, MI 48109-2118, U.S.A.

Abstract

The effect of initial flow conditions on the primary breakup of nonturbulent and turbulent liquid jets in still gases was studied experimentally. Pressure-atomized jets were provided by a piston/cylinder arrangement followed by a converging passage to yield nonturbulent slug flow. The degree of flow development at the jet exit was controlled by removing the boundary layer formed on the converging passage, and providing constant-diameter passages of various lengths after boundary layer removal. Test conditions included water, n-heptane and various glycerol mixtures injected into helium, air and Freon 12 at pressures of 1 and 2 atm. Pulsed photography and holography were used to observe the liquid surface prior to primary breakup. The results highlight the importance of liquid vorticity at the jet exit on primary breakup: experiments with nearly vorticity-free exit conditions (passage length/diameter ratio, L/d = 0.15) caused primary breakup to be suppressed, yielding stable liquid jets similar to those used in liquid jet cutting processes. In contrast, larger L/d at sufficiently high Reynolds numbers caused transition to turbulent jets having wrinkled surfaces prior to primary breakup by the turbulent primary breakup mechanism. A breakup regime map was developed, yielding behavior in the turbulent primary breakup regime for L/d > 4-6 and passage Reynolds numbers > 1-4 × 10^4. Within the turbulent primary breakup regime, conditions for the onset of breakup, and the evolution of drop sizes with distance from the jet exit, all were relatively independent of L/d for values up to 212. Finally, a new correlation for drop sizes after primary breakup at nonturbulent conditions was developed, based on consideration of boundary layer thicknesses at the jet exit.

Nomenclature

C_{NT}	=	experimental constant
d	=	jet exit diameter
d_p	=	drop diameter
L	=	constant diameter passage length
L_p	=	converging passage length
MMD	=	mass median drop diameter
Oh_d	=	jet exit Ohnesorge number ($= \mu_f/(\rho_f d\sigma)^{1/2}$
Re_{fd}	=	jet exit Reynolds number ($= \rho_f d\ \bar{u}_o/\mu_f$
Re_{fx}	=	Reynolds number based on distance from the jet exit
SMD	=	Sauter mean diameter
$\bar{u}_o$	=	mean jet exit velocity
We_{ij}	=	Weber number based on density of phase i and length scale j ($= \rho_j \bar{u}_o^2/\sigma$)
x	=	distance from jet exit
Λ	=	radial spatial integral scale of turbulence
μ	=	molecular viscosity
ρ	=	density
σ	=	surface tension
Subscripts		
f	=	liquid phase property
FD	=	fully-developed condition
g	=	gas phase property
i	=	at point of breakup initiation

INTRODUCTION

An experimental study of the effects of initial flow conditions on the properties of dispersed liquid generation (primary breakup) along the surfaces of liquid jets in still gases is described. The research was motivated by the importance of primary breakup to the structure and mixing properties of the near-injector (dense spray) region of pressure-atomized sprays. Measurements were made of effects of jet exit conditions on the onset of primary breakup and on drop size distributions after primary breakup. The experiments involved both nonturbulent and turbulent round-jet exit conditions for noncavitating flows within the liquid passage. Effects of physical properties were studied by considering a range of liquids (water, n-heptane and various glycerol mixtures) and ambient gas environments (air, helium and Freon 12 at pressures of 1 and 2 atm.). The study was limited, however, to primary breakup along the surface of liquid jets in the second wind-induced and atomization breakup regimes,[1,2] as opposed to breakup of the entire liquid column itself.

Many investigators have reported significant effects of jet exit conditions on the atomization properties of pressure-atomized sprays in still gases, see Refs. 3-23, among others. In particular, the early studies of De Juhasz et al.[3] and Lee and Spenser[4] showed that atomization quality differed for laminar and turbulent jet exit conditions. Subsequently, Phinney[5] and Grant and Middleman[6] found that jet stability and the onset of breakup were affected by the presence of turbulence at the jet exit. In fact, more recent work shows that jet exit conditions dominate atomization properties for pressure atomization at large liquid/gas density ratios, typical of injection in air at atmospheric pressure. For example, Hoyt and Taylor[8-10] observed little effect of relative velocities on primary breakup when jet exit conditions were turbulent, for relative velocities comparable to injection velocities. Finally, Arai et al.[11-13] and Karasawa et

*Research Fellow, currently with AMC, P.O. Box 33830, WPAFB, OH 45433-0830.
†Visiting Researcher, from Department of Mechanical Engineering, University of Uberlandia, Uberlandia M. G., Brazil.
**Professor, Fellow AIAA.

al.[14] showed that breakup could be suppressed entirely for super-cavitating flows where the liquid jet separates from the injector passage wall, and does not reattach, to yield a relatively uniform and nonturbulent flow at the jet exit. In retrospect, this behavior is not surprising because jet exit conditions of this type are widely used for liquid jet cutting systems, where avoiding breakup is a major design objective.[15]

A series of studies in this laboratory have helped to quantify some effects of jet exit conditions and aerodynamic forces on the properties of pressure atomization in still gases.[16-23] Jet exit conditions involved either nonturbulent slug flow, or fully-developed turbulent pipe flow, with gamma-ray absorption and pulsed holography used to measure distributions of liquid volume fractions and drop sizes after primary breakup. It was found that mixing rates were faster, the length of the potential-core-like liquid column near the jet exit was reduced, and drop sizes after primary breakup were increased, for turbulent rather than nonturbulent jet exit conditions.[16-20] A more surprising finding was that long accepted aerodynamic stripping theories of primary breakup[24-26] were not effective.[21-23] For liquid/gas density ratios greater than 500, drop sizes after nonturbulent primary breakup were successfully correlated by assuming that they were proportional to the thickness of boundary layers formed along liquid surface waves with no direct consideration of aerodynamic effects.[21] Similarly, for liquid/gas density ratios greater than 500, drop sizes after nonturbulent primary breakup were successfully correlated by phenomenological analysis considering effects of surface tension and liquid turbulence properties alone.[22,23] Aerodynamic effects were observed for turbulent primary breakup at lower liquid/gas density ratios, however, they could be explained as a result of merging of primary breakup and secondary breakup with the latter treated based on recent results for the secondary breakup of drops.[27,28]

Thus, existing measurements of primary breakup properties have been dominated by effects of vorticity and turbulence at the jet exit.[19-23] Available information about nonturbulent breakup, however, has been limited to a single injector passage while liquid/gas density ratios less than 500, where aerodynamic effects might be expected, have not been explored. Additionally, study of turbulent primary breakup has been limited to injector passage length-to-diameter ratios, $L/d > 40$, at high Reynolds numbers in order to yield fully-developed turbulent pipe flows at the jet exit;[29,30] therefore, the range of L/d and passage Reynolds numbers needed to reach this regime has not been resolved. Thus, the present investigation sought to address these gaps in the literature, with the following specific objectives: (1) to investigate effects of passage properties and liquid/gas density ratios on drop sizes after nonturbulent primary breakup; and (2) to investigate effects of L/d and passage Reynolds numbers on onset conditions for turbulent primary breakup and drop sizes after turbulent primary breakup. The experiments involved relatively large diameter (3.6-9.5 mm) nonevaporating liquid jets injected into still gases to provide liquid/gas density ratios in the range 104-7240. This simplified the control of jet exit conditions while including conditions where aerodynamic effects might be expected ($\rho_f/\rho_g < 500$). Similar to past work,[21-23] drop size distributions after primary breakup were measured using pulsed holography. As noted earlier, observations were limited to breakup along the surface of the liquid jet from the jet exit , rather than breakup of the entire liquid jet itself.

The article begins with a description of experimental methods. Results for nonturbulent breakup are then discussed, considering flow visualization, phenomenological analysis to find drop sizes after primary breakup, and the correlation of measurements and predictions. The paper concludes with discussion of results for turbulent primary breakup, considering flow visualization, a turbulent breakup regime map, and the effects of jet exit conditions on the onset and drop sizes after turbulent primary breakup.

EXPERIMENTAL METHODS

Apparatus

The test apparatus was similar to the arrangement used by Wu and Faeth[23] and will be described only briefly. It consisted of a pneumatically-driven piston/cylinder arrangement containing a 600 ml sample of the liquid to be injected. The outlet of the cylinder had a rounded contraction to prevent cavitation as illustrated in Fig. 1. The profile of the contraction was designed according to Smith and Wang[31] to provide a uniform velocity (slug flow) across the exit, aside from boundary layers along the walls of the passage. Acceptable performance of these designs was established earlier for steady operation using laser velocimetry.[16,17] Detailed measurements of the turbulence properties of the present contraction sections have not been made but turbulence levels are expected to be low because conditions at the start of the contraction section are relatively quiescent and the contraction ratio is large (roughly 100:1). Injection was vertically downward within a windowed test chamber, with the liquid collected at the bottom of the chamber and then discarded.

Tests of nonturbulent, slug flow injection involved terminating the flow passage at the end of the contraction section. Tests of turbulent injection, and to identify the regimes of turbulent primary breakup, involved following the contraction section with a constant-diameter passage as illustrated in Fig. 1. In this case, the diameter of the injector exit was smaller than the diameter of the outlet of the contraction, so that boundary layers formed along the walls of the contraction section could be removed by the sharp leading edge (cutter) of the constant-diameter section. This provided a well defined slug flow inlet condition for the constant-diameter section with flow properties at the exit of this section controlled by its length. Thus, jet exit conditions ranged from nonturbulent slug flow ($L/d = 0.15$) to fully-developed turbulent pipe flow for sufficiently large L/d and passage Reynolds numbers.

The windowed test chamber was cylindrical with a diameter of 300 mm and a length of 1370 mm. The chamber could be evacuated and refilled with various gases at pressures of 1 and 2 atm. in order to change liquid/gas density ratios while avoiding problems of cavitation and flashing at low chamber pressures. Instrumentation was mounted rigidly; therefore, various distances from the jet exit were considered by traversing the injector within the test chamber while horizontal positions were varied by traversing the entire injector/chamber assembly.

The piston/cylinder arrangement was filled with test liquid as described earlier.[21-23] Test operation was initiated by admitting high-pressure air to the upper side of the piston through a solenoid valve which forced the liquid through the jet passage. Total test times were short, 200-10000 ms, however,

this was sufficient due to short flow development and data acquisition times. Jet exit velocities at the time of the measurements were calibrated using an impact plate, similar to Refs. 21-23.

Instrumentation

Instrumentation consisted of pulsed shadowgraph photography and pulsed holography, using the same arrangements and methods as Refs. 21-23. Pulsed shadowgraph photography was used to measure primary breakup properties near the onset of breakup, to measure the streamwise location of the onset of breakup, and to identify the type of primary breakup. The holocamera was used for this purpose, operating in the single-pulse mode with the reference beam blocked to yield a shadowgraph rather than a hologram. Experimental uncertainties (95% confidence) of the location of the onset of breakup were less than 40%, similar to Refs. 22, 23; this is relatively large due to the angular variation of ligaments protruding from the surface and the randomness of drop separation from the tips of ligaments.

Single-pulse holography was used for drop diameter determinations, using a configuration and methods of image analysis identical to Refs. 21-23. Drop size distributions, the mass median diameter (MMD) and the Sauter mean diameter (SMD) were found by summing over 40-200 objects at each condition. Experimental uncertainties of these properties were dominated by finite sampling limitations because primary breakup yields relatively few drops, particularly near the onset of breakup. Thus, experimental uncertainties (95% confidence) of MMD and SMD are estimated to be only less than 40%, comparable to Refs. 21-23.

Test Conditions

Test conditions for nonturbulent and turbulent jets are summarized in Tables 1 and 2, respectively. Present data for nonturbulent jets were supplemented by earlier measurements from Refs. 17,18,20 and 21 using similar injector designs based on Smith and Wang[31] profiles for the contraction sections to yield a nonturbulent slug flow at the jet exit. Present data for the turbulent jets were supplemented by earlier measurements from Refs. 17,18,20,22 and 23; in these cases, a rounded contraction section was directly followed by a constant diameter section with no boundary layer removal but with $L/d > 40$ to yield fully-developed turbulent pipe flow at the jet exit for sufficiently large passage Reynolds numbers.

Both nonturbulent (Table 1) and turbulent (Table 2) jet experiments involved injection of water, n-heptane or various glycerol mixtures into still helium, air or Freon 12 at pressures of 1 or 2 atm. This provided a variety of liquid properties with liquid/gas density ratios in the range 104-7420 so that aerodynamic effects could be assessed. Injector diameters were in the range 3.6-9.5 mm in order to vary boundary layer properties on the injector passage walls for nonturbulent jets, and the integral scales of turbulence for the turbulent jets (Similar to past work,[22,23] streamwise and radial integral scales at the jet exit will be taken to be 0.4d and d/8, respectively, based on the measurements of Laufer for fully-developed turbulent pipe flow as cited by Hinze.[30]). Jet exit velocities were in the range 1.7-134 m/s, yielding gas Mach numbers less than 0.4; therefore, effects of compressibility were small. Effects of gas type on surface tension were small for present conditions as well, so that the values used in Tables 1 and 2 were specifically based on measurements in air at atmospheric pressure.

Jet exit velocities for nonturbulent jets (Table 1) were in the range 16-134 m/s, yielding the following ranges of jet and primary breakup dynamic parameters: Re_{fd} of 17,000-750,000, We_{gd} of 19-2,750 and Oh_d of 0.0011-0.018. Except for a few test conditions in helium, $We_{gd} > 40$ and $We_{fd} > 8$, which places present measurements in the atomization breakup regime for nonturbulent liquids defined by Miesse[1] and Ranz,[2] where primary breakup should begin at the jet exit.

Jet exit velocities for the turbulent jets (Table 2) were in the range 1.7-99 m/s, yielding the following ranges of jet and primary breakup dynamic parameters: Re_{fd} of 5,600-780,000, We_{gd} of 0.29-1160, We_{fd} of 250-653,000 and Oh_d of 0.0011-0.020. Overall, these conditions span the Rayleigh, wind-induced and atomization breakup regimes of Refs. 1 and 2; however, present measurements will specifically address issues of the mode of breakup and its onset.

NONTURBULENT JETS

Flow Visualization

Consideration of the experimental results will begin with nonturbulent jets, in order to highlight the importance of vorticity in the liquid at the jet exit for primary breakup over the present test range. The importance of vorticity at the jet exit is illustrated by the pulsed shadowgraph photographs of the liquid jet near the jet exit appearing in Fig. 2. Two injector conditions are shown: one involving nonturbulent slug flow leaving the contraction section without removal of the boundary layers near the passage walls, the other involving the same contraction section and flow rate but with the boundary layer removed by a cutter followed by a short constant area section ($L/d = 0.15$). In both cases, water was injected into still room air at atmospheric pressure. When the cutter is absent, ligaments form very close to the jet exit shortly followed by breakup of their tips to form drops according to the nonturbulent primary breakup mechanism considered in Ref. 21. In contrast, when the boundary layers at the passage exit are removed by the cutter, followed by a short constant-diameter section which prevents significant development of subsequent boundary layers along the passage walls, primary breakup along the liquid surface is entirely suppressed. In this case, a solid liquid stream, similar to those used for liquid cutting jets,[15] was observed, which only involved the appearance of relatively large scale surface irregularities (sinuous and helical waves) at $x/d > 30$.

The behavior seen in Fig. 2, where primary breakup is inhibited when the flow at the jet exit is nearly uniform and nonturbulent, is consistent with past observations of effects of jet exit and aerodynamic conditions on primary breakup. In particular, Arai et al.[11-13] and Karasawa et al.[14] observe the suppression of primary breakup for injection into still air for supercavitating injector flows, where supercavitation in the injector passage prevents the development of vorticity within the liquid jet somewhat analogous to the action of the cutter during the present experiments. Additionally, recent study of primary breakup of turbulent liquids injected into still gases suggests relatively small aerodynamic effects for liquid/gas density ratios greater than 500,[23] like the results illustrated in Fig. 2. This was confirmed by repeating these experiments with injection into

a helium environment, where the substantial increase of the liquid/gas density ratio should act to suppress aerodynamic effects.[23] In spite of this change, however, the behavior of primary breakup when the cutter was not used was very similar to the results illustrated in Fig. 2. Thus, for conditions involving nonturbulent jets over the present test range, vorticity generated in the injector passage dominates the primary breakup process and the aerodynamic effects considered by the classical aerodynamic breakup theories[24-26] appear to be negligible.

Drop Properties

Other preliminary measurements confirmed general observations concerning nonturbulent primary breakup from Wu et al.[21] First of all, it was found that drop size distributions after primary breakup satisfied the universal root normal distribution with MMD/SMD = 1.2, proposed by Simmons.[32] Since this is a two-parameter distribution function, fixing the ratio MMD/SMD implies that the complete size distribution can be defined by a single parameter, which will be taken to be the SMD in the following. Additionally, the SMD after primary breakup increased with distance from the injector for a time before becoming relatively independent of distance from the injector in a fully-developed nonturbulent primary breakup regime for $\rho_f x \bar{u}_o/\mu_f > 10^6$, see Ref. 21. The fully-developed breakup regime dominated primary breakup properties for present test conditions; therefore, subsequent considerations will be limited to these conditions, similar to Ref. 21.

As a result of these observations, the phenomenological analysis for drop sizes after nonturbulent breakup due to Wu et al.,[21] loosely based on aerodynamic stripping ideas, was modified to account for the dominant effect of liquid vorticity at the jet exit. The general nature of the new approach is illustrated in Fig. 3. The boundary layer of length L_p, which forms along the contraction section of the injector, is assumed to create the vortical liquid region responsible for primary breakup. Additionally, the drop sizes resulting from primary breakup, represented by the SMD, are assumed to be proportional to the thickness of the boundary layer at the jet exit. Finally, it is assumed that the boundary layer thickness at the jet exit scales in the same manner as a laminar flat plate boundary layer for an ambient velocity $\bar{u}_o$ and a length L_p.[29] These assumptions imply:

$$SMD_{FD}/L_p \sim (\mu_f/(\rho_f L_p \bar{u}_o))^{1/2} \qquad (1)$$

It is convenient to rearrange Eq. (1) so that We_{gSMD} and Re_d are introduced, because this facilitates comparison with earlier correlations and evaluation of potential secondary breakup effects. Completing this rearrangement yields:

$$We_{gSMD} = C_{NT}(L_p/d)^{1/2} We_{gd}/Re_d^{1/2} \qquad (2)$$

where C_{NT} is an empirical constant involving various proportionality factors. When interpreting Eq. (2), it should be recalled that properties like the gas density, the surface tension and the jet exit diameter have been introduced arbitrarily and that aerodynamic stripping plays no role in the proposed mechanism of nonturbulent primary breakup, i.e., that drop sizes after primary breakup are taken to be proportional to the thickness of the vorticity-containing region at the jet exit as represented by Eq. (1).

The form of Eq. (2) was tested by combining the present measurements with those of Refs. 17,18 and 20, as summarized in Table 1. The resulting correlation of all the measurements is illustrated in Fig. 4. The correlation of the data for all the liquids, ambient gas environments, jet exit velocities and jet exit diameters is seen to be remarkably good. The power of the correlation in terms of the independent variable is not unity as suggested by Eq. (2), however, and can be represented better by the following empirical fit, that is shown on the plot;

$$We_{gSMD} = 7.0[(L_p/d)^{1/2} We_{gd}/Re_d^{1/2}]^{0.87} \qquad (3)$$

The standard deviations of the constant and power of Eq. (3) are 2 and 3%, respectively, while the correlation coefficient of the fit is 0.99—which is excellent. The reduction of the power of the independent variable on the right hand side of Eq. (3) from unity to 0.87 is statistically significant but is not large in view of the qualitative development of the correlation. However, this reduction helps to account for relatively modest reductions of the SMD with increasing gas density observed during present measurements and those of Tseng et al.,[20] i.e., $SMD \sim \rho_g^{-0.13}$ from Eq. (3). Thus, a small aerodynamic contribution to nonturbulent primary breakup may be involved in the reduction of the power as well.

The correlation of Eq. (3) also was evaluated using results reported by Hoyt and Taylor.[9] This involved analyzing a photograph of breakup appearing in this paper, selecting drops near the liquid surface for x/d in the range 7-9, which is within tthe fully-developed regime. The liquid passage in this case had a conical contraction section with a 7° half angle and a contraction ratio of 4.2, followed by a constant area section having L/d = 1. The measurement yielded an SMD of 430 μm, while Eq. (3) yields SMD_{FD} of 530 μm. In view of the rather different liquid passage configurations, and the limited accuracy and extent of the measurements, this level of agreement is encouraging. Nevertheless, Eq. (3) should not be used for the developing region of nonturbulent primary breakup, where drop sizes generally are smaller,[21] and it should be recalled that the expression was tested mianly for injectors having Smith and Wang[31] profiles for the contraction section. Finally, conditions for the onset of this breakup regime have not been identified. Thus, much remains to be done to gain a better understanding of how primary breakup occurs due to nonturbulent vortical regions in the flows at the jet exit.

The limits of secondary breakup are illustrated in Fig. 4, assuming that relative drop velocities after primary breakup can be approximated by $\bar{u}_o$ and that the drop size distribution function satisfies the universal root normal distribution function. The first approximation is reasonable based on measurements of drop velocities after nonturbulent primary breakup which show that the largest drops, that are most likely to experience secondary breakup, have relative velocities nearly equal to the mean jet exit velocity.[17,18,20] Next, it is generally agreed that drops are unstable to secondary breakup when their Weber number, $We_{gp} > 13$, see Hsiang and Faeth[27,28] and references cited therein. Finally, the universal root normal distribution implies that drop diameters within three standard deviations of the MMD have the diameter range $0.098 \le d_p/SMD \le 3.5$ and contain 99.7% of the spray mass. These assumptions imply that We_{gSMD} = 1.8 and 66 define limiting conditions where virtually no drops or all drops undergo secondary breakup. Noting that it is difficult to remain in the atomization breakup

regime for values of $We_{gd}/Re_{fd}^{1/2}$ much lower than the present test range, it is clear from the results illustrated in Fig. 4 that nonturbulent primary breakup yields sprays that should involve *significant levels of secondary breakup.*

TURBULENT JETS

Flow Visualization

Injector passage design, including the inlet contraction, the presence of trips and other turbulence promoting devices, and the roughness and length of the constant area section, all can modify conditions required for turbulent flow (and its degree of development) at the jet exit;[29,30] correspondingly, this affects conditions required for the presence of turbulent primary breakup. Thus, in order to control the number of test variables, present considerations were limited to conditions where either the boundary layer formed on the contraction section was removed, and the resulting slug flow was passed through constant area sections of given L/d (for $L/d \leq 10$), or where the contraction section was immediately followed by a relatively long constant area passage (for $L/d \geq 40$).

For present passage configurations, the onset of turbulent primary breakup was affected by both the L/d ratio of the constant area section of injector passage and the Reynolds number of the flow through the injector passage. The effect of L/d is illustrated by typical pulsed photographs of the flow near the jet exit illustrated in Fig. 5. Three conditions are shown: contraction section boundary layer removal (cutter) with $L/d = 4$, a cutter with $L/d = 10$ and a round contraction followed by a long constant area section with $L/d = 41$. Passage Reynolds numbers for all three conditions exceed 10^5, which is sufficient to obtain fully-developed turbulent pipe flow for sufficiently long L/d.[29,30] In fact, normal turbulent primary breakup, with an irregular liquid surface near the jet exit followed by the formation of irregular ligaments and drops farther downstream, is observed for $L/d = 41$, which corresponds to conditions considered during earlier studies of turbulent primary breakup.[17,18,20-23] On the other hand, the liquid surface remains smooth near the jet exit and no breakup is observed for $L/d = 4$, yielding behavior similar to the findings for a short cutter discussed in connection with Fig. 2. Increasing the length of the constant area section to $L/d = 10$, however, yields a turbulent primary breakup process very similar to observations with large L/d passages.

The effect of the passage Reynolds number on the onset of turbulent primary breakup is illustrated in Fig. 6. In this case, a 42% glycerol mixture was injected at progressively increasing velocities to yield passage Reynolds numbers of 1.5, 2.0, 3.3 and 4.2×10^4 with $L/d = 7$. At the two lowest Reynolds numbers, the liquid surface at the jet exit is smooth, followed by the appearance of sinuous waves and then large-scale irregular breakup: this behavior will be called sinuous jets in the following. With increasing Reynolds number, there is a tendency for the irregular or turbulent-like portion of the breakup process to merge with, and eventually precede, the sinuous wave portion of the flow, disrupting the sinuous waves. Finally, at sufficiently high Reynolds numbers, the liquid surface becomes roughened close to the jet exit and the flow exhibits the properties of turbulent primary breakup.

Breakup Regime Map

Conditions for the appearance of laminar, sinuous and turbulent jets are summarized as a function of L/d and Re_{fd} in Fig. 7. Observations of laminar and sinuous jets are denoted by cross-hatched, half-darkened and darkened symbols. In addition to the present results, earlier observations of Refs. 17,20,22 and 23, using rounded inlets followed by relatively large L/d constant area sections ($L/d \geq 40$) are shown on the plot. Finally, the observations of Grant and Middleman[6] are shown on the figure, they involve sharp edged inlets which promote caviation at the inlet to the constant area section, and were more disturbed than the other measurements.

The flow regimes illustrated in Fig. 7 for the Smith and Wang[31] contractions yield transition to laminar jets when L/d becomes smaller than 4-6, independent of Re_{fd} up to the largest values considered (10^6). For $L/d > 6$, transition between sinuous and turbulent jets is observed in the range $Re_{fd} = 1\text{-}4 \times 10^4$, with a general tendency for Re_{fd} at transition to become smaller as L/d increases. This behavior can be anticipated from the well known tendency for large L/d passages to exhibit turbulent flow at their exit at lower Reynolds numbers.[33] Finally, the relatively large values of Reynolds numbers for turbulent pipe flow ($Re_{fd} \geq 10^4$) are typical of behavior observed by others for relatively disturbance-free inlet conditions.[32]

The observations of Grant and Middleman[6] illustrated in Fig. 7 highlight the potential effects of inlet disturbances. In particular, their observations for somewhat disturbed inlets indicate transition to turbulent jets at a Reynolds number of roughly 3,000, which is comparable to the lowest Reynolds numbers where turbulent pipe flow has been observed.[29,30] The results of Arai et al.[11-13] also suggest that the transition to laminar jets at $L/d = 4\text{-}6$ may be reduced for highly disturbed inlet conditions due to the presence of cavitation bubbles, e.g., they observed jet exit flows typical of turbulent jets for $L/d = 4$ using square or slightly rounded inlet contractions at sufficiently high Reynolds numbers. This behavior probably is due to the development of turbulent regions near points of reattachment of cavity flows which act to trip turbulent flows even in relatively short passages. Thus, present estimates of the turbulent breakup regime are somewhat conservative and are representative of relatively disturbance-free slug flows at the inlet of the constant area section. As noted earlier, effects of disturbances at the inlet, as well as separated flows and effects of inlet cavitation, offer a rich area of study that merits attention; however, such considerations are beyond the scope of the present study.

The final issue with respect to breakup regimes involves the influence of aerodynamic effects on transition to the turbulent primary breakup regime. Present measurements considered these effects for a gas density range of 0.16-9.63 kg/m^3. The corresponding range of liquid/gas density ratios was 104-7240, with aerodynamic effects influencing drop sizes after turbulent primary breakup regime for liquid/gas density ratios less than 500.[23] Nevertheless, no effect of liquid/gas density ratio on transition to the turbulent primary breakup regime was observed for the present test range. This is reasonable because the onset of turbulent jet conditions appears to be dominated by effects of transition within the constant area section of the jet passage.

Onset of Turbulent Primary Breakup

In addition to defining the turbulent primary breakup regime, it also is of interest to determine drop sizes at the onset of breakup along the liquid surface, and the distance from the jet exit where breakup begins. Earlier work considered these issues for fully-developed turbulent pipe flow at the jet exit ($L/d \geq 40$).[22,23] The objective of the present measurements was to evaluate effects of L/d within the turbulent primary breakup regime. Since aerodynamic effects had proven to be relatively uninteresting with respect to conditions needed to reach the turbulent primary breakup regime, only liquid/gas density ratios greater than 500 were considered, where aerodynamic effects on turbulent primary breakup are small.[23]

Earlier work involved use of phenomenological analysis to find the drop sizes and the location of turbulent primary breakup.[22,23] Drops at the onset condition were assumed to be formed from the smallest turbulent eddy whose kinetic energy, relative to the surrounding fluid, was sufficient to provide the required surface energy of a comparable-sized drop, for conditions where aerodynamic effects were small.[22] The location of the onset of primary breakup was then found from the distance required for this critical eddy to move from the jet exit in order to form a drop as a result of Rayleigh breakup of the corresponding protruding eddy-sized ligament.[22] These considerations yielded the following best-fit correlations for SMD_i and x_i, based on earlier measurements where aerodynamic effects were small:[22]

$$SMD_i/\Lambda = 133\ We_{f\Lambda}^{-0.74} \qquad (4)$$

$$x_i/\Lambda = 3980\ We_{f\Lambda}^{-0.67} \qquad (5)$$

Corresponding expressions when aerodynamic effects are significant ($\rho_f/\rho_g < 500$) can be found in Ref. 23.

Similar to past studies of turbulent primary breakup,[22,23] drop size distributions always satisfied the universal root normal distribution function, with MMD/SMD = 1.2, of Simmons;[32] therefore, drop sizes will be described by the SMD alone in the following. Measurements of the SMD_i are plotted according to the variables of Eq. (4) in Fig. 8; the correlation of Eq. (4) also appears on the plot. Results are shown for L/d = 10, 41 and 121, all for sufficiently high Reynolds numbers to be within the turbulent primary breakup regime. These results include present measurements using a cutter inlet to the constant area section with L/d = 10, as well as earlier measurements Refs. 20, 22 and 23 where a rounded inlet was immediately followed by constant area passages, with L/d = 41 and 121. It is seen that there is a consistent trend for the SMD_i when L/d = 10 to be somewhat larger than results when L/d = 41 and 121. This seems reasonable because the turbulence spectrum is not well developed near the transition condition, at small L/d, which limits the availability of small-scale eddies;[30] this effect will be discussed further when the evolution of drop sizes with distance from the jet exit is considered. Nevertheless, in view of the experimental uncertainties of the SMD_i, the effect of reduced L/d is not large. Thus, it is reasonable to use the correlation of Eq. (4), as well as the corresponding correlation from Ref. 23 when aerodynamic effects are significant, throughout the turbulent primary breakup regime.

Measurements of x_i are correlated according to the variables of Eq. (5) in Fig. 9; the correlation of Eq. (5) also appears on the plot. The conditions of the measurements are similar to those for SMD_i except that present results include observations at both L/d = 7 and 10, the former value being near the lower limit of the turbulent primary breakup regime, see Fig. 7. Similar to the results for SMD_i, variations of x_i over the present range of L/d are small in comparison to experimental uncertainties. Thus, it seems reasonable to use Eq. (5), as well as the corresponding correlation from Ref. 23 when aerodynamic effects are significant, throughout the turbulent primary breakup regime.

Drop Sizes After Primary Breakup

The last issue to be considered is the effect of L/d on the evolution of drop sizes after turbulent primary breakup with distance from the jet exit. For conditions where aerodynamic effects are not important, the variation of drop sizes with distance was found by assuming that drop sizes at a given location correspond to the size of ligaments completing Rayleigh breakup to form drops from their tips at the same position.[22] These considerations yielded the following best fit correlation for SMD as a function of x, based on earlier measurements where aerodynamic effects were small:[22]

$$SMD/x = 0.69[x/(\Lambda\ We_{f\Lambda}^{1/2})]^{2/3} \qquad (6)$$

Corresponding results where aerodynamic effects are significant ($\rho_f/\rho_g < 500$) involve merging of primary and secondary breakup; the correlation for SMD as a function of x in this case can be found in Ref. 23.

Measurements of SMD as a function of x are correlated according to the variables of Eq. (6) in Fig. 10; the correlation of Eq. (6) also appears on the plot. Present measurements for L/d = 10 are shown on the figure, along with earlier results for L/d = 41, 121 and 212 from Refs. 17,18,20,22 and 23. All these results involve conditions where aerodynamic effects are small. Results for L/d = 10 for values of $x/(\Lambda\ We_{f\Lambda}^{1/2}) > 4 \times 10^{-2}$ generally are comparable to earlier measurements at larger L/d; thus, for these conditions Eq. (6) provides a correlation for the SMD, within experimental uncertainties, throughout the turbulent primary breakup regime. For smaller values of $x/(\Lambda\ We_{f\Lambda}^{1/2})$, however, the measured SMD for L/d = 7 are consistently larger than the results at larger L/d. This behavior is reminiscent of effects of L/d seen for SMD_i in Fig. 7. The smallest (Kolmogorov) scales of fully-developed turbulence were an order of magnitude smaller than present measurements of SMD in this region ($\ell_K/SMD_i \approx 0.03$-$0.06$). Thus, incomplete development of the turbulence spectrum, which is expected near conditions where transition to turbulence occurs,[29,30] provides the most promising explanation for larger SMD than expected from Eq. (6) near the onset of turbulent primary breakup at small L/d. Other features of Fig. 10, including the core length of Grant and Middleman,[6] are discussed in Ref. 22. Finally, turbulent primary breakup yields larger drops than nonturbulent primary breakup at comparable conditions; therefore, turbulent primary breakup has larger potential for secondary breakup than indicated earlier for nonturbulent primary breakup.

CONCLUSIONS

Primary breakup near the jet exit region of large-scale pressure-atomized sprays in still gases was studied, emphasizing effects of jet exit conditions on the primary breakup process. The major conclusions of the study were as follows:

1. Jet exit conditions, particularly the presence of vorticity due to turbulence or variations of mean velocities from viscous effects in boundary layers, play a dominant role in primary breakup along the surfaces of liquid jets in gases.

2. Nonturbulent slug flows, with boundary layers formed prior to the jet exit removed, did not undergo breakup along the surface of the liquid jet but formed intact liquid jets similar to those used in liquid cutting jets and observed by Arai et al.[11-13] and Karasawa et al.[14] for supercavitating injectors with no reattachment of the liquid jet to the passage walls.

3. Nonturbulent slug flows undergo nonturbulent primary breakup and yield drop sizes that correlate with the thickness of boundary layers at the passage walls near the jet exit, see Fig. 4 and Eq. (3).

4. The turbulent primary breakup regime, for nonturbulent slug flow with boundary layer removal at the inlet to the constant-diameter section, involves $L/d > 4\text{-}6$ and $Re_{fd} > 1.4 \times 10^4$, independent of aerodynamic effects, see Fig. 7.

5. More disturbed conditions at the inlet of the constant area section increases the range of conditions where turbulent primary breakup can be observed; for example turbulent primary breakup was observed by Grant and Middleman[6] at Re_{fd} ca. 3000 and large L/d, and by Arai et al.[11-13] at $L/d = 4$ and large Re_{fd}, for sharp-edged inlets that caused cavitation disturbances at the inlet.

6. Within the turbulent primary breakup regime, conditions at the onset of turbulent primary breakup, SMD_i and x_i, and the subsequent variation of SMD after primary breakup with distance from the jet exit, are relatively independent of L/d; thus, Eqs. (4), (5) and (6) are recommended for these properties when aerodynamic effects are small, along with corresponding equations from Ref. 23 when aerodynamic effects must be considered, see Figs. 8-10.

Present results are mainly limited to conditions where Smith and Wang[31] profiles are used to yield nonturbulent slug flows at the exit of the converging section. Effects of changing the geometry of the contraction section, as well as the presence of trips, other turbulence generating devices, and reattached flows after cavitation or separation bubbles, merit further consideration due to the widespread presence of such conditions for practical injectors.

Acknowledgments

The research was sponsored by the Office of Naval Research, grant no. N00014-89-J-1199, under the technical management of G. D. Roy. Initial development of instrumentation was sponsored by the Air Force Office of Scientific Research, grant no. 89-0516 with J. M. Tishkoff serving as Technical Manager. The U.S. Government is authorized to reproduce and distribute copies for governmental purposes notwithstanding any copyright notation thereon.

REFERENCES

[1]C.C. Miesse, "Correlation of Experimental Data on the Disintegration of Liquid Jets," Ind. Engr. Chem., Vol. 47, 1955, pp. 1690-1697.

[2]W.E. Ranz, "Some Experiments on Orifice Sprays," Can. J. Chem. Engr., Vol. 36, 1958, pp. 175-181.

[3]K.J. De Juhasz, O.F. Zahm, Jr. and P.H. Schweitzer, "On the Formation and Dispersion of Oil Sprays," Bulletin No. 40, Engineering Experimental Station, Pennsylvania State University, University Park, PA, 1932, pp. 63-68.

[4]D.W. Lee and R.C. Spencer, "Preliminary Photomicrographic Studies of Fuel Sprays," NACA Tech. Report 424, 1933.

[5]R.E. Phinney, "The Breakup of a Turbulent Jet in a Gaseous Atmosphere," J. Fluid Mech., Vol. 88, 1966, pp. 119-127.

[6]R.P. Grant and S. Middleman, "Newtonian Jet Stability," AIChE J., Vol. 12, 1966, pp. 669-678.

[7]M.J. McCarthy and N.A. Malloy, "Review of Stability of Liquid Jets and the Influence of Nozzle Design," Chem. Engr. J., Vol. 7, 1974, pp. 1-20.

[8]J.W. Hoyt and J.J. Taylor, "Turbulence Structure in a Water Jet Discharging in Air," Phys. Fluids, Vol. 20, Pt. II, 1977, pp. S253-S257.

[9]J.W. Hoyt and J.J. Taylor, "Waves on Water Jets," J. Fluid Mech., Vol. 88, 1977, pp. 119-123.

[10]J.W. Hoyt and J.J. Taylor, "Effect of Nozzle Boundary Layer on Water Jets Discharging in Air, *Jets and Cavities*," J.H. Kim, O. Furuya and B.R. Parkin, eds., ASME-FED, Vol. 31, ASME, New York, 1985., pp. 93-100.

[11]M. Arai, M. Shimizu and H. Hiroyasu, "Break-Up Length and Spray Angle of High Speed Jet," Proceedings of the 3rd International Conference on Liquid Atomization and Spray Systems, 1985, pp. IB/4/1-IB /4/10.

[12]M. Arai, M. Shimizu and H. Hiroyasu, "Break-Up Length and Spray Formation Mechanisms of a High Speed Liquid Jet," Proceedings of the 4th International Conference on Liquid Atomization and Spray Systems, 1988pp. 177-184.

[13]H. Hiroyasu, M. Arai and M. Shimizu, "Break-Up Length of a Liquid Jet and Internal Flow in a Nozzle," Proceedings of the 5th International Conference on Liquid Atomization and Spray Systems, 1991, pp. 275-282.

[14]T. Karasawa, M. Tanaka, K. Abe, S. Shiga and T. Kurabayashi, "Effects of Nozzle Configuration on the Atomization of a Steady Spray," Atom. Sprays, Vol. 2, No. 4, 1992, pp. 411-426.

[15]M. Yokota, Y. Ito and T. Shinoke, "High Speed Photographic Observations of Cavitation Arising in the High-Speed Oil-Flow Through a Very Small Long Orifice," 9th International Symposium on Jet Cutting Technology, Sendai, Japan, 1988, pp. 13-21.

[16]G.A. Ruff, A.D. Sagar and G.M. Faeth, "Structure and Mixing Properties of Pressure-Atomized Sprays," AIAA J., Vol. 27, No. 7, 1989, pp. 901-908.

[17]G.A. Ruff, L.P. Bernal and G.M. Faeth, "Structure of the Near-Injector Region of Non-Evaporating Pressure-Atomized Sprays," J. Prop. Power, Vol. 7, No. 2, 1991, pp. 221-230.

[18]G.A. Ruff, P.-K. Wu, L.P. Bernal and G.M.Faeth, "Continuous- and Dispersed-Phase Structure of Dense Non-Evaporating Pressure-Atomized Sprays," J. Prop. Power, Vol. 8, No. 2, 1992, pp. 280-289.

[19]L.-K. Tseng, G.A. Ruff and G.M. Faeth, "Effects of Gas Density on the Structure of Liquid Jets in Still Gases," AIAA J., Vol. 30, No. 6, 1992, pp. 1537-1544.

[20]L.-K. Tseng, P.-K. Wu and G.M. Faeth, "Dispersed-Phase Structure of Pressure-Atomized Sprays at Various Gas Densities," J. Prop. Power, Vol. 8, No. 6, 1992, pp. 1157-1166.

[21]P.-K. Wu, G.A. Ruff and G.M. Faeth, "Primary Breakup in Liquid/Gas Mixing Layers," Atom. Sprays, Vol. 1, No. 4, 1991, pp. 421-440.

[22]P.-K. Wu, L.-K. Tseng and G.M. Faeth, "Primary Breakup in Gas/Liquid Mixing Layers for Turbulent Liquids," Atom. Sprays, Vol. 2, No. 3, 1992, pp. 295-317.

[23]P.-K. Wu and G.M. Faeth, "Aerodynamic Effects in Primary Breakup of Turbulent Liquids," Atom. Sprays, Vol. 3, 1993, pp. 265-289.

[24]G.I. Taylor, "Generation of Ripples by Wind Blowing Over a Viscous Liquid," *The Scientific Papers of Sir Geoffrey Ingram Taylor*, Vol. III, G.K. Batchelor, ed., Cambridge University Press, Cambridge, England, 1963, pp. 244-254.

[25]V.G. Levich, *Physicochemical Hydrodynamics*, Prentice-Hall, Inc., Englewood Cliffs, NJ, 1962, pp. 639-646.

[26]R.D. Reitz and F.V. Bracco, "Mechanism of Atomization of a Liquid Jet," Phys. Fluids, Vol. 25, 1982, pp. 1730-1742.

[27]L.-P. Hsiang and G.M. Faeth, "Near-Limit Drop Deformation and Secondary Breakup," Int. J. Multiphase Flow, Vol. 18, No. 5, 1992, pp. 635-652.

[28]L.-P. Hsiang and G.M. Faeth, "Drop Properties After Secondary Breakup," Int. J. Multiphase Flow, Vol. 19, No. 5, 1993, pp. 721-735.

[29]H. Schlichting, *Boundary Layer Theory*, 7th ed., McGraw-Hill, New York, 1979, p. 599.

[30]J.O. Hinze, *Turbulence*, 2nd ed., McGraw-Hill, New York, 1975, 1975, pp 427 and 724-742.

[31]R.M. Smith and C.-T. Wang, "Contracting Cones Giving Uniform Throat Speeds," J. Aero. Sci., Vol. 11, 1944, pp. 356-360.

[32]H.C. Simmons, "The Correlation of Drop-Size Distributions in Fuel Nozzle Sprays," J. Engr. Power, Vol. 99, 1977, pp. 309-319.

[33]A.M.O. Smith, "Remarks on Transition in a Round Tube," J. Fluid Mech., Vol. 7, Pt. 4, 1960, pp. 565-576.

Table 2 Test Conditions for Turbulent Jets[a]

Liquid	Water[b,c]	n-Heptane[b]	Glycerol[b] (42%)	Glycerol (63%)
ρ_f (kg/m^3)	997	683	1101	1158
ρ_g (kg/m^3)	0.16-9.63	1.15	1.15	0.16-9.63
ρ_f/ρ_g	104-623	594	957	120-7240
L/d	0.15-212	41	7-41	7-121
d (mm)	3.6-9.5	6.4	4.0-6.4	4.0-6.4
$\bar{u}_o$ (m/s)	1.7-99	20-45	13-99	16-76
$Re_{fd} \times 10^{-3}$	10-780	220-500	16-200	5.6-45
We_{gd}	0.29-1005	154-778	12-1160	3.9-1090
$We_{fd} \times 10^{-3}$	0.25-552	8.7-44	11-109	18-653
$Oh_d \times 10^3$	1.09-1.77	1.10	5.23-6.58	16.2-20.2

[a]Pressure-atomized injection vertically downward in still gases at 298 ± 3 K.
[b]Data includes results from Wu et al.[22,23]
[c]Data includes results from Ruff et al.[17,18] and Tseng et al.[20]

Table 1 Test Conditions for Nonturbulent Jets[a]

Gas	Helium	Air	Freon 12 (1 atm)	Freon 12 (2 atm)
ρ_g (kg/m^3)	0.16	1.15-4.68	4.68	9.63
ρ_f (kg/m^3)	997	683-1158	997	997
ρ_f/ρ_g	6230	213-1007	213	104
d (mm)	6.0	5.0[b],6.0,9.5[c]	6.0	6.0
$\bar{u}_o$ (m/s)	37-71	16-134	37-71	37,58
$Re_{fd} \times 10^{-3}$	250-480	17-750	250-480	250,390
We_{gd}	19-68	74-1490	540-2000	1120,2750
$We_{fd} \times 10^{-3}$	120-430	490-12600	120-430	120,480
$Oh_d \times 10^3$	1.4	1.1-18.1	1.4	1.4

[a]Pressure-atomized injection vertically downward in still gases at 298 ± 3 K. L_p = 35, 35 and 32 mm for d = 5.0, 6.0 and 9.5 mm, respectively.
[b]Data from Wu et al.[21]
[c]Data from Ruff et al.[17,18] and Tseng et al.[20]

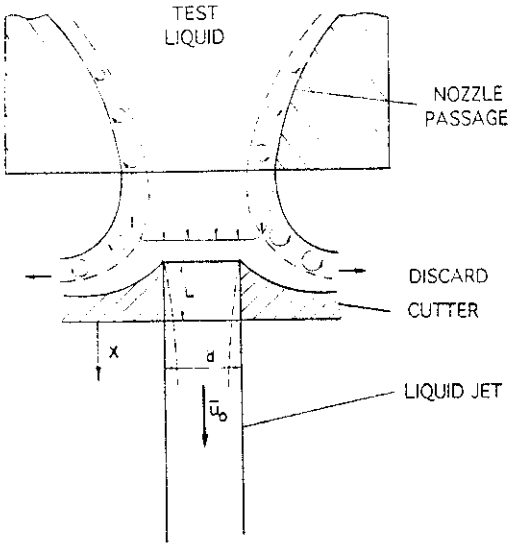

Fig. 1 Sketch of the jet exit arrangement.

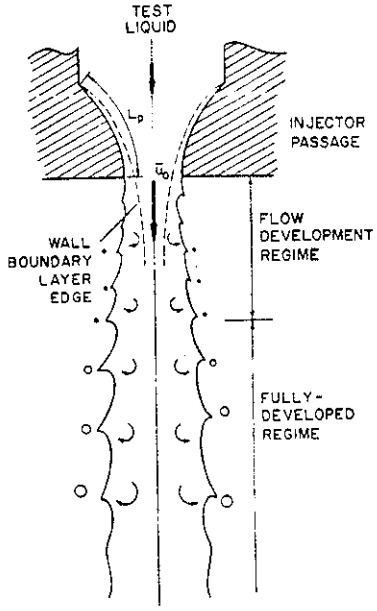

Fig. 3 Sketch of the injector passage vorticity mechanism for nonturbulent primary breakup.

Fig. 2 Jet appearance with and without boundary layer removal for nonturbulent slug flow.

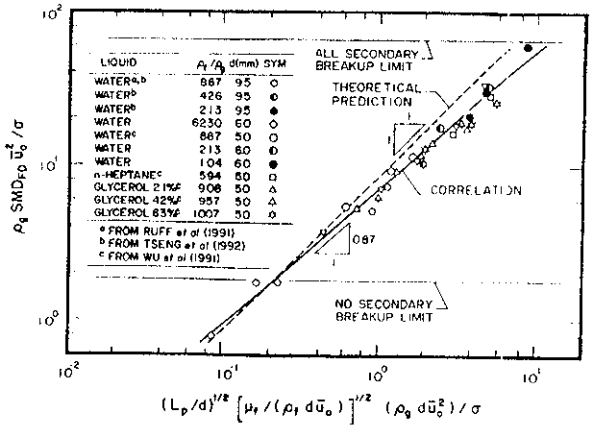

Fig. 4 Correlation of SMD_{FD} based on the injector passage boundary layer vorticity mechanism .

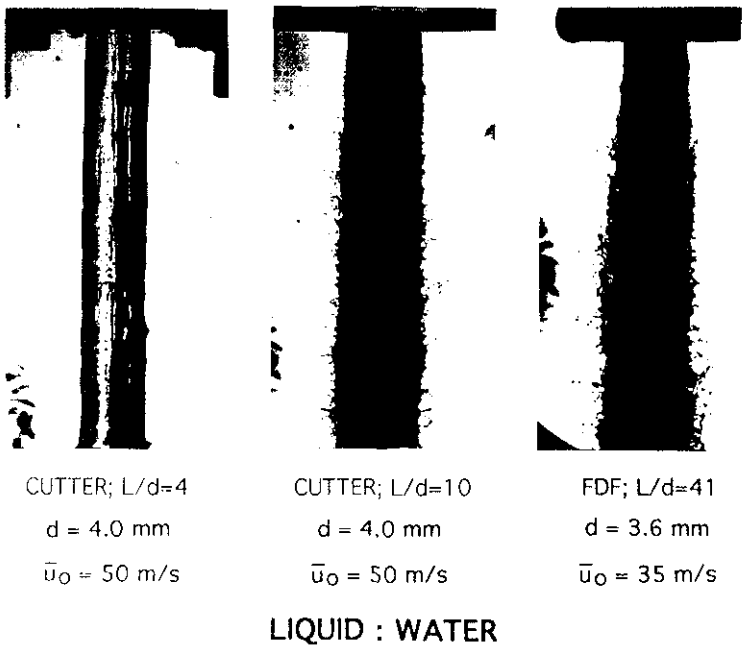

Fig. 5 Pulsed photographs of liquid jets for various L/d.

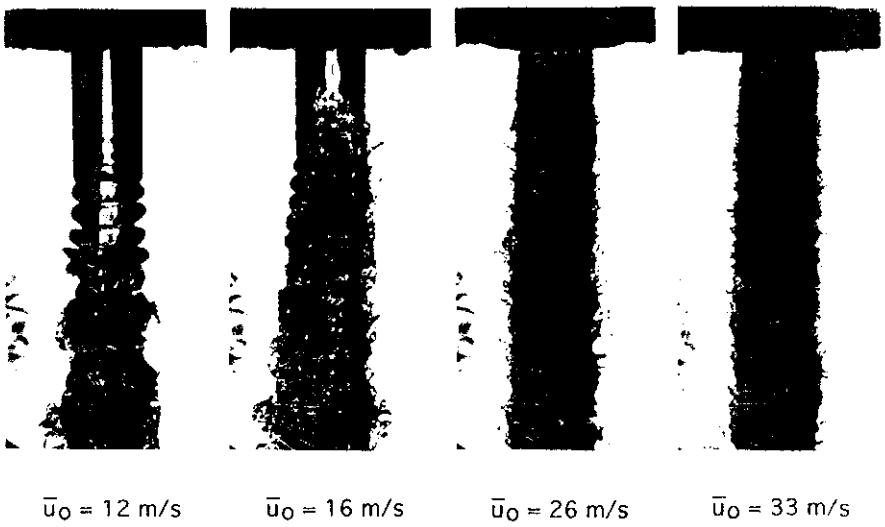

Fig. 6 Pulsed photographs of liquid jets for various $\bar{u}_o$.

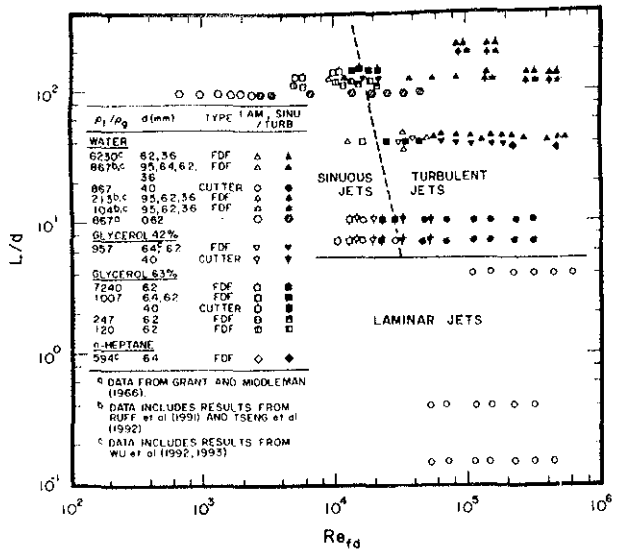

Fig. 7 Breakup regime map.

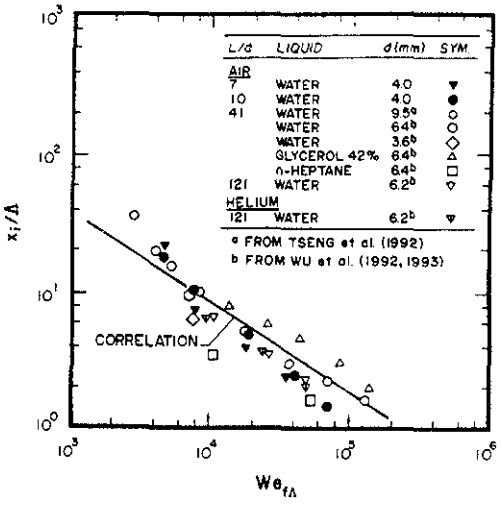

Fig. 9 Location of the onset of breakup.

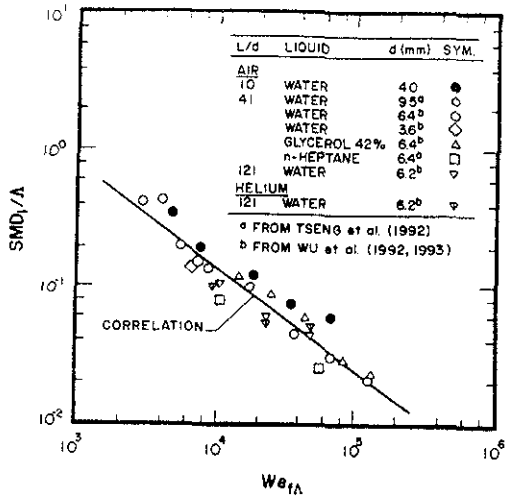

Fig. 8 SMD at the onset of breakup.

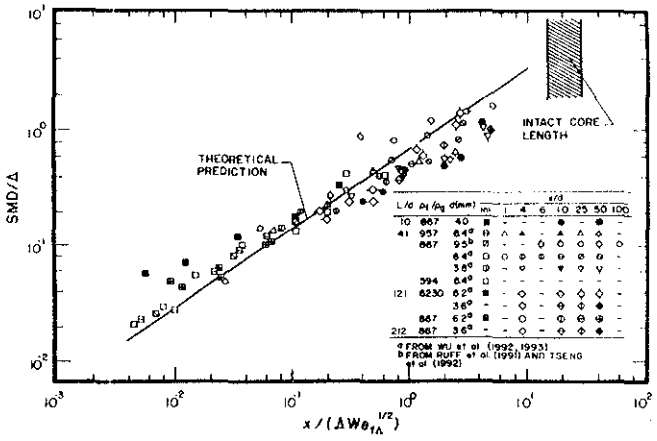

Fig. 10 Effect of L/d and streamwise distance on drop sizes after turbulent primary breakup.